Localization and delocalization of light in photonic moiré lattices

Peng Wang,[1] Yuanlin Zheng,[1] Xianfeng Chen,[1] Changming Huang,[2] Yaroslav
V. Kartashov,[3,4] Lluis Torner,[3,5] Vladimir V. Konotop,[6] Fangwei Ye[1*]

[1] *School of Physics and Astronomy, Shanghai Jiao Tong University, Shanghai 200240, China*

[2]*Department of Electronic Information and Physics,*

Changzhi University, Shanxi 046011, China

[3]*ICFO-Institut de Ciencies Fotoniques, The Barcelona Institute of Science and Technology,*

08860 Castelldefels (Barcelona), Spain

[4]*Institute of Spectroscopy, Russian Academy of Sciences, Troitsk, Moscow, 108840, Russia*

[5]*Universitat Politecnica de Catalunya, 08034 Barcelona, Spain*

[6]*Departamento de Física, and Centro de Física Teórica e Computacional,*

Faculdade de Ciências, Universidade de Lisboa,

Campo Grande, Ed. C8, Lisboa 1749-016, Portugal

[*]*Corresponding author: fangweiye@sjtu.edu.cn*

(Dated: August 28, 2019)

Moiré lattices consist of two identical periodic structures overlaid with a relative rotation angle. Present even in everyday life, moiré lattices have been also produced, e.g., with coupled graphene-hexagonal boron nitride monolayers [1, 2], graphene-graphene layers [3, 4], and layers on a silicon carbide surface [5]. The recent surge of interest in moiré lattices arises from the possibility to explore in such systems a rich variety of outstanding physical phenomena, such as commensurable-incommensurable transitions and topological defects [2], emergence of insulating states due to band flattening [3, 6], unconventional superconductivity [4] controlled by the rotation angle [7, 8], quantum Hall effect [9], realization of non-Abelian gauge potentials [10], quasicrystals appearing at special rotation angles [11], to name only a few examples. A fundamental question that remains unexplored is the evolution of waves in the potentials defined by the moiré lattices. Here we experimentally create two-dimensional photonic moiré lattices, which, unlike their material predecessors, have readily controllable parameters and symmetry allowing to explore transitions between structures with fundamentally different geometries: periodic, general aperiodic, and quasi-crystal ones. Equipped with such realization, we observe localization of light in deterministic linear lattices. Such localization is based on flat-band physics [6], in contrast to previous schemes based on light diffusion in optical quasicrystals [12], where disorder is required [13] for the onset of Anderson localization [16]. Using commensurable and incommensurable moiré patterns, we report the first experimental demonstration of two-dimensional localization-delocalization-transition (LDT) of light. Moiré lattices may feature almost arbitrary geometry that is consistent with the crystallographic symmetry groups of the sublattices, and therefore afford a powerful tool to control the properties of light patterns, to explore the physics of transitions between periodic and aperiodic phases, and two-dimensional wavepacket phenomena relevant to several areas of science.

One of the most salient properties of an engineered optical system is its capability to affect a light beam in a prescribed manner, such as to control its diffraction pattern or to localize it. The importance of wavepacket localization extends far beyond optics and impacts all branches of science dealing with wave phenomena. Homogeneous or strictly periodic linear systems cannot result in wave localization, the latter requiring presence of structure defects or nonlinearity. Wave localization in random media, or Anderson localization [17], is a hallmark discovery of condensed-matter physics. All electronic states in one- and two-dimensional potentials with uncorrelated disorder are localized. Three-dimensional systems with disordered potentials are known to have both localized and delocalized eigenstates [16], separated by an energy known as the mobility edge [18]. Coexistence of localized and delocalized eigenstates has been predicted also in regular quasiperiodic one-dimensional systems, first in the discrete Aubry-André [19] model and later in continuous optical and matter-wave systems [20–22]. Quasiperiodic (or aperiodic) structures, even those that possess long-range order, fundamentally differ both from periodic systems, where all eigenmodes are delocalized Bloch waves, and from disordered media, where all states are localized (in one or two dimensions). Upon variation of the parameters of a quasiperiodic system, it is possible to observe the transition between localized and delocalized states. Such LDT has been observed in one-dimensional quasiperiodic optical [23] and in atomic systems [24, 25].

Wave localization is sensitive to the dimensionality of the physical setting. Anderson localization and mobility edge in two-dimensional disordered systems were first reported in experiments with bending waves [26] and later in optically induced disordered lattices [27]. In quasicrystals localization has been observed only under the action of nonlinearity [12] and in the presence of strong disorder [13]. Although localization and delocalization of light in two-dimensional systems without any type of disorder and nonlinearity have been predicted theoretically for moiré lattices [14] and very recently for Vogel spirals [15], the phenomenon has never been observed experimentally.

Here we report the first experimental realization of reconfigurable photonic moiré lattices with controllable parameters and symmetry. The lattices are induced by two superimposed periodic patterns [28, 29] (sublattices) with either square or hexagonal primitive cells. They

3

have tunable amplitudes and twist angle. Depending on the twist angle, a photonic moiré lattice may have different periodic (commensurable) structure or aperiodic (incommensurable) structure without translational periodicity, but they always feature the rotational symmetry of the sublattices. Moiré lattices can also transform into quasicrystals with higher rotational symmetry [11]. The angles at which a commensurable phase (periodicity) of a moiré lattice is achieved are determined by Pythagorean triples in the case of square sublattices [14], or by another Diophantine equation when the primitive cell of the sublattices is not a square (see Methods). For all other rotation angles the structure is aperiodic albeit regular (i.e., it is not disordered). Changing the relative amplitudes of the sublattices allows to smoothly tune the shape of the lattice without affecting its rotational symmetry.

In contrast to crystalline moiré lattices [1–5], optical patterns are monolayer structures, i.e., both sublattices interfere in one plane. As a consequence, light propagating in such media is described by a one-component field. In the paraxial approximation, the propagation of an extraordinary polarized beam in a photorefractive medium with an optically induced refractive index is governed by the Schrödinger equation for the dimensionless field amplitude $\psi(\mathbf{r}, z)$ [30]:

$$i\frac{\partial \psi}{\partial z} = -\frac{1}{2}\nabla^2 \psi + \frac{E_0}{1 + I(\mathbf{r})}\psi. \tag{1}$$

Here $\nabla = (\partial/\partial x, \partial/\partial y)$; $\mathbf{r} = (x, y)$ is the radius-vector in the transverse plane scaled to the wavelength $\lambda = 632.8$ nm of the beam used in the experiments; z is the propagation distance scaled to the diffraction length $2\pi n_e \lambda$; n_e is the refractive index of the homogeneous crystal for extraordinary-polarized light; $E_0 > 0$ is the dimensionless applied dc field; $I(\mathbf{r}) \equiv |p_1 V(\mathbf{r}) + p_2 V(S\mathbf{r})|^2$ is the moiré lattice induced by two ordinary-polarized mutually coherent periodic sublattices $V(\mathbf{r})$ and $V(S\mathbf{r})$ interfering in the (x, y) plane and rotated by the angle θ with respect to each other (see Methods); $S = S(\theta)$ is the operator of the two-dimensional rotation; p_1 and p_2 are the amplitudes of the first and second sublattices, respectively. The number of laser beams creating each sublattice $V(\mathbf{r})$ depends on the desired lattice geometry. The form in which the lattice intensity $I(\mathbf{r})$ enters Eq. (1) is determined by the mechanism of the photorefractive response.

To visualize the formation of moiré lattices it is convenient to associate a continuous

4

sublattice $V(\mathbf{r})$ with a discrete one with lattice vectors determined by the locations of the absolute maxima of $V(\mathbf{r})$. The resulting moiré pattern inherits the rotational symmetry of $V(\mathbf{r})$. At specific angles some nodes of different sublattices may coincide thereby leading to translational symmetry of the moiré pattern in commensurable phase, see primitive translation vectors illustrated by blue arrows in Fig. 1 (the first and third columns) and Fig. 4 (the first and second columns) for square and honeycomb sublattices, respectively. The rotation angles at which the periodicity of $I(\mathbf{r})$ is achieved are determined by triples of positive integers $(a, b, c) \in \mathbb{Z}^+$ related by a Diophantine equation characteristic for a given sublattice [14] (see Extended Data Tab. I).

First, we consider a Pythagorean lattice created by two square sublattices. For the rotation angles θ, such that $\cos\theta = a/c$ and $\sin\theta = b/c$, where (a, b, c) is a Pythagorean triple, i.e., $a^2 + b^2 = c^2$, $I(\boldsymbol{r})$ is a periodic moiré lattice. Such angle is referred below as Pythagorean. For all other, non-Pythagorean, rotation angles θ, the lattice $I(\boldsymbol{r})$ is aperiodic. Figures 1(a)-(c) compare calculated $I(\boldsymbol{r})$ patterns (first row) with lattices created experimentally [30] in a biased SBN:61 photorefractive crystal with dimensions $5 \times 5 \times 20$ mm^3 (third row) for different rotation angles. The second row shows the respective discrete moiré lattices. Columns (a) and (c) show periodic lattices, while column (b) gives an example of an aperiodic lattice. All results were obtained for $E_0 = 7$, which corresponds to a 8×10^4 V/m dc electric field applied to the crystal. The amplitude of the first sublattice was set to $p_1 = 1$ in all cases, which corresponds to an average intensity $I_{\mathrm{av}} \approx 3.8$ mW/cm^2. For such parameters, the refractive index modulation depth in the moiré lattice is of the order of $\delta n \sim 10^{-4}$.

Mathematically, incommensurable lattices are almost periodic functions [32]. Any non-Pythagorean twist angle can be approached by a Pythagorean one with any prescribed accuracy (see Supplementary Information). Thus, any finite area of an incommensurable moiré lattice can be approached by a primitive effective cell of some periodic Pythagorean lattice, while a more accurate approximation requires a larger primitive cell of the Pythagorean lattice. This property is illustrated in Fig. 1(d,e) by the quantitative similarities between the densities of states (DOSs) calculated for an incommensurable lattice and its effective-cell approximation. A remarkable property of Pythagorean lattices is the extreme flattening of

5
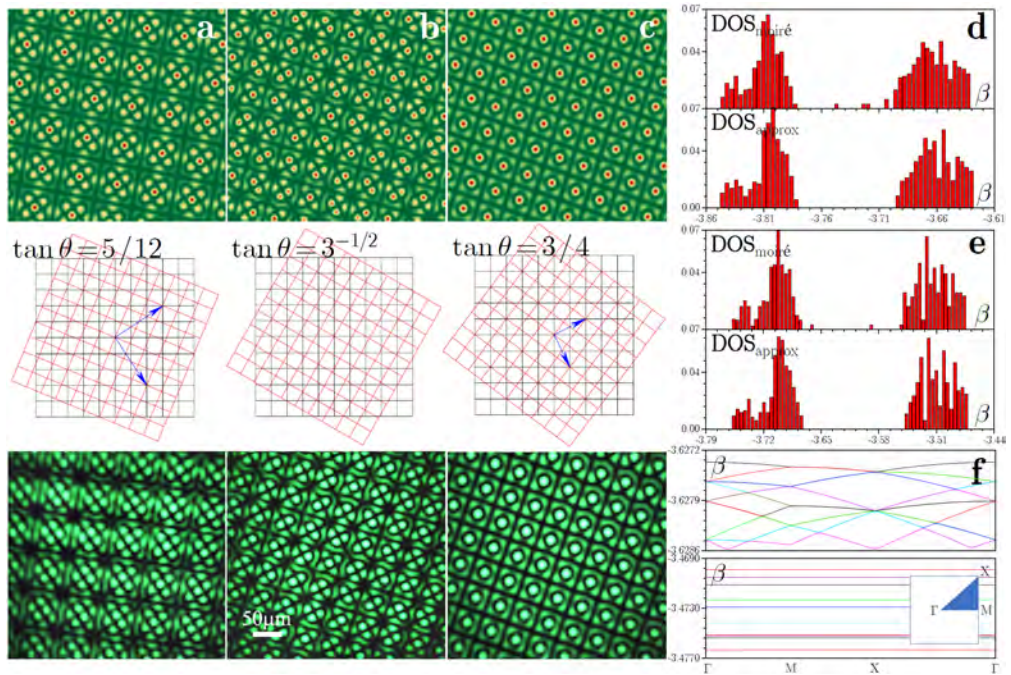
FIG. 1: (a)-(c) Moiré lattices $I(\boldsymbol{r})$ generated by two interfering square sublattices with $p_1 = p_2$, whose axes are mutually rotated by the angle indicated in each panel. First row: calculated patterns. Second row: schematic discrete representation of two rotated sublattices. Third row: experimental patterns at the output face of the crystal. The scale is the same for all images. Comparison of DOS calculated for moiré lattice (top) and its periodic approximation (bottom) at $p_2 = 0.1$ (d) and $p_2 = 0.2$ (e). The approximate Pythagorean lattice has period $b_1 = \sqrt{3361}\pi$ (see Supplementary Information). (f) Band structures for periodic lattice approximating moiré lattice at $p_2 = 0.1$ (top, 15 upper bands are shown) and $p_2 = 0.2$ (bottom, 68 upper bands are shown). In all cases $p_1 = 1$.

the higher bands that occurs when the ratio p_2/p_1 exceeds a certain threshold [Fig. 1(f)]. The number of flat bands grows with the size of the area of the primitive cell of the Pythagorean lattice approximation. Thus, an incommensurable moiré lattice can be viewed as the large-area limit of a periodic Pythagorean lattice with extremely flat higher bands. Note that existence of flat bands for twisted bilayer graphene was earlier discussed in [7, 8, 31]. Since flat bands support quasi-nondiffracting localized modes, an initially localized beam launched

6

into such moiré lattice will remain localized. This flat-band physics of moiré lattices, fundamentally different from that of Anderson localization in random media, allows us to predict light localization above a threshold value of the ratio p_2/p_1. Furthermore, flat bands support states that are exponentially localized in the primitive cell and that can be well approximated by exponentially localized two-dimensional Wannier functions [33] (see Fig. 2(c) and Supplementary Information).

To elucidate the impact of the sublattice amplitudes and rotation angle θ on the light localization, we calculated the linear eigenmodes $\psi(\boldsymbol{r}, z) = w(\boldsymbol{r})e^{i\beta z}$, where β is the propagation constant and $w(\boldsymbol{r})$ is the mode profile, supported by the moiré lattices. To characterize their localization we use the integral form-factor $\chi = [U^{-2} \iint |\psi|^4 d^2\boldsymbol{r}]^{1/2}$, where $U = \iint |\psi|^2 d^2\boldsymbol{r}$ is the energy flow (the integration is over the transverse area of the crystal). The form-factor is inversely proportional to the mode width: the larger the value of χ, the stronger the localization. The dependence of the form-factor of the most localized mode (the mode with largest β) on θ and p_2 is shown in Fig. 2(a) (for modes with lower values of β the dependencies are qualitatively similar). One observes a sharp LDT above a certain threshold depth p_2^{LDT} of the second sublattice, at the amplitude of the first sublattice $p_1 = 1$. Below p_2^{LDT} all modes are extended [Fig. 2(b)] and above the threshold, some modes are localized [Fig. 2(c)]. This is consistent with the extreme band flattening of the approximate Pythagorean lattice at $p_2 > p_2^{\mathrm{LDT}}$ [Fig. 1(f)]. The inset in Fig. 2(c) reveals exponential tails for $p_2 > p_2^{\mathrm{LDT}}$ from which the localization length for the most localized mode can be extracted.

Figure 2(a) shows delocalization for angles θ set by the Pythagorean triples, when all modes are extended regardless of the value of p_2. It also reveals that p_2^{LDT} is practically independent of the non-Pythagorean rotation angle. This is explained by the fact that a large fraction of the power in a localized mode resides in the vicinity of a lattice maximum (i.e., at $\boldsymbol{r} = \boldsymbol{0}$). In an incommensurable phase $I(\boldsymbol{r}) < I(\boldsymbol{0})$ for all $\boldsymbol{r} \neq \boldsymbol{0}$ the optical potential can be approximated by the Taylor expansion of $E_0/[1 + I(\boldsymbol{r})]$ with respect to $\boldsymbol{r}$ near the origin. Such expansion includes the rotation angle θ only in the fourth order (see Supplementary Information), and locally can be viewed as almost isotropic.

To study the guiding properties of the Pythagorean moiré lattices experimentally we mea-
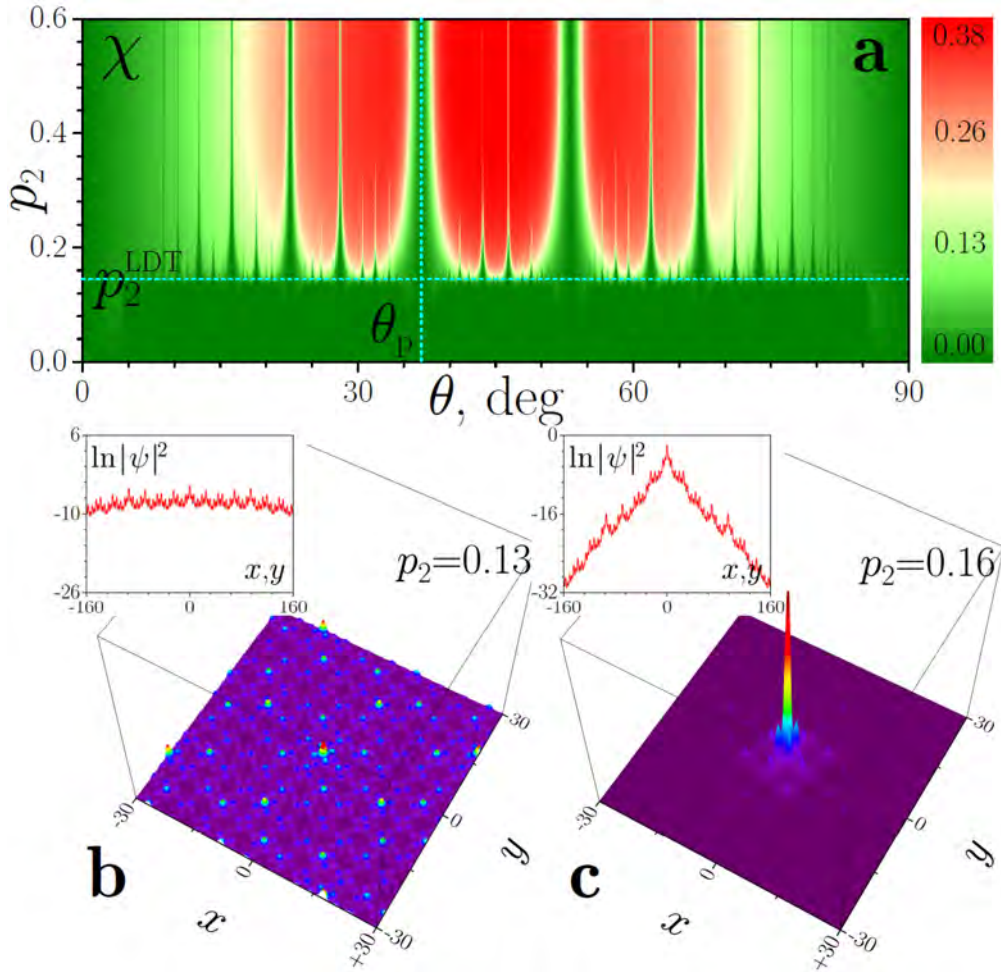
FIG. 2: (a) Form-factor (inverse width) of the eigenmodes with largest β versus rotation angle θ and versus amplitude of the second sublattice p_2 at $p_1 = 1$. The horizontal dashed line indicates the sublattice depth p_2^{LDT} at which LDT occurs. The vertical dashed line shows one of the Pythagorean angles $\theta_{\mathrm{p}} = \arctan(3/4)$. Examples of mode profiles with largest β for $p_2 < p_2^{\mathrm{LDT}}$ (b) and $p_2 > p_2^{\mathrm{LDT}}$ (c). Insets show cuts of $\ln|\psi|^2$ distribution along the x and y axes.

sured the diffraction outputs for beams propagating in lattices corresponding to different rotation angles θ for fixed input position of the beam, centered or off-center. The diameter of the Gaussian beam focused on the input face of the crystal was about 23 μm. Such a beam covers approximately one bright spot (channel) of the lattice profile. The intensity of the input beam was about 10 times lower than the intensity of the lattice-creating beam,

8

I_{av}, to guarantee that the beam does not distort the induced refractive index and that it propagates in the linear regime.
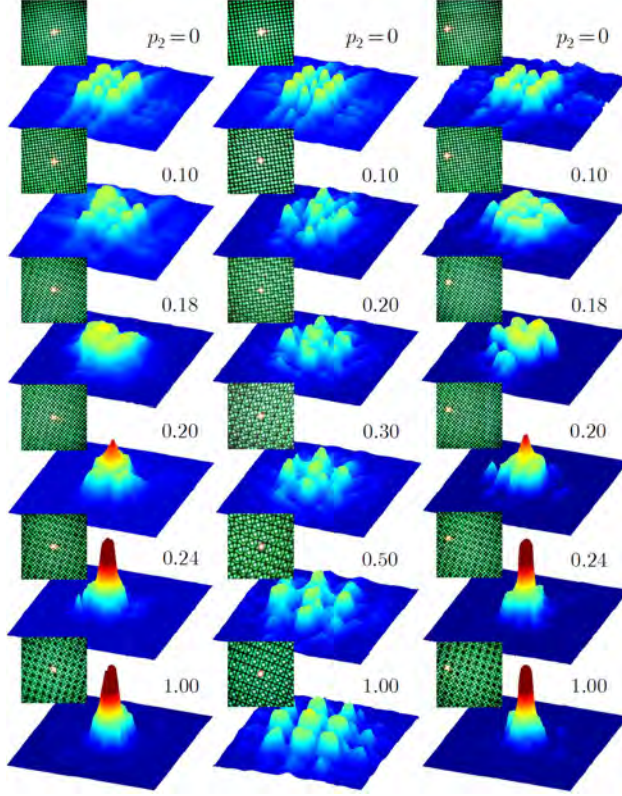
FIG. 3: Observed output intensity distributions illustrating LDT with increasing amplitude p_2 of the second sublattice for rotation angle $\theta = \arctan 3^{-1/2} = \pi/6$ (left and right columns) and absence of LDT for the Pythagorean angle $\theta = \arctan(3/4)$ (central column). The insets show the location of the excitation, namely: central for the left and central columns, and off-center for the right column.

Experimental evidence of LDT in the two-dimensional lattice is presented in Fig. 3, where we compare output patterns for the low-power light beam in the incommensurable ($\tan\theta = 3^{-1/2}$, left and right columns for central and off-center excitations, respectively) and commensurable ($\tan\theta = 3/4$, central column) moiré lattices, tuning in parallel the amplitude p_2 of the second sublattice. When $p_2 < p_2^{\mathrm{LDT}}$ (in Fig. 3 $p_2^{\mathrm{LDT}} \approx 0.15$), the light beam in the incommensurable lattice notably diffracts upon propagation and expands across multiple

local maxima of $I(\boldsymbol{r})$ in the vicinity of the excitation point. However, when p_2 exceeds the LDT threshold, it is readily visible that diffraction is arrested for both central (left column) and off-center (right column) excitations and a localized spot is observed at the output over a large range of p_2 values. In clear contrast, localization is absent for any p_2 value in the periodic lattice associated with the Pythagorean triple (central column). Additional proof of the LDT is reported in Extended Data Fig. 1. We compare experimental and theoretical results for propagation at $p_1 = 1$. In an incommensurable lattice at $p_2 < p_2^{\mathrm{LDT}}$ one observes beam broadening (top row). Localization takes place at $p_2 > p_2^{\mathrm{LDT}}$ (middle row). At a Pythagorean twist angle localization does not occur even for $p_2 = p_1 = 1$ (bottom row). Simulations of the propagation up to much larger distances beyond the available sample length presented in Extended Data Fig. 2 confirm localization of the beam in incommensurable lattice at any distance at $p_2 > p_2^{\mathrm{LDT}}$ and its expansion at $p_2 < p_2^{\mathrm{LDT}}$.

The mutual rotation of two identical sublattices allows generation of commensurable and incommensurable moiré patterns with sublattices of any allowed symmetry. To illustrate the universality of LDT, we induced hexagonal moiré lattices. The technique of induction is similar to that used for single honeycomb photonic lattices [34]. For such lattices, the rotation angles producing commensurable patterns are given by the relation $\tan\theta = b\sqrt{3}/(2a + b)$, where the integers a and b solve the Diophantine equation $a^2 + b^2 + ab = c^2$. Two examples are presented in the first and second columns of Fig. 4. In such periodic structures, the light beam experiences considerable diffraction for any amplitude of the sublattices, as shown in the bottom row. To observe LDT one has to induce aperiodic structures. To such end, we set the rotation angle to 30°. In such incommensurable case we did observe LDT by increasing the amplitude of the second sublattice, keeping the amplitude p_1 fixed. Delocalized and localized output beams are shown in the lower panels of the third and fourth columns of Fig. 4. In the third column the ideal 6-fold rotation symmetry of the output pattern is slightly distorted, presumably due to the intrinsic anisotropy of the photorefractive response. At $p_2 = p_1$ the moiré pattern acquires a 12-fold rotational symmetry (shown in the fourth column of Fig. 4) as proposed in [11] as a model of a quasicrystal and similar to the twisted bilayer graphene quasicrystal reported in [5].
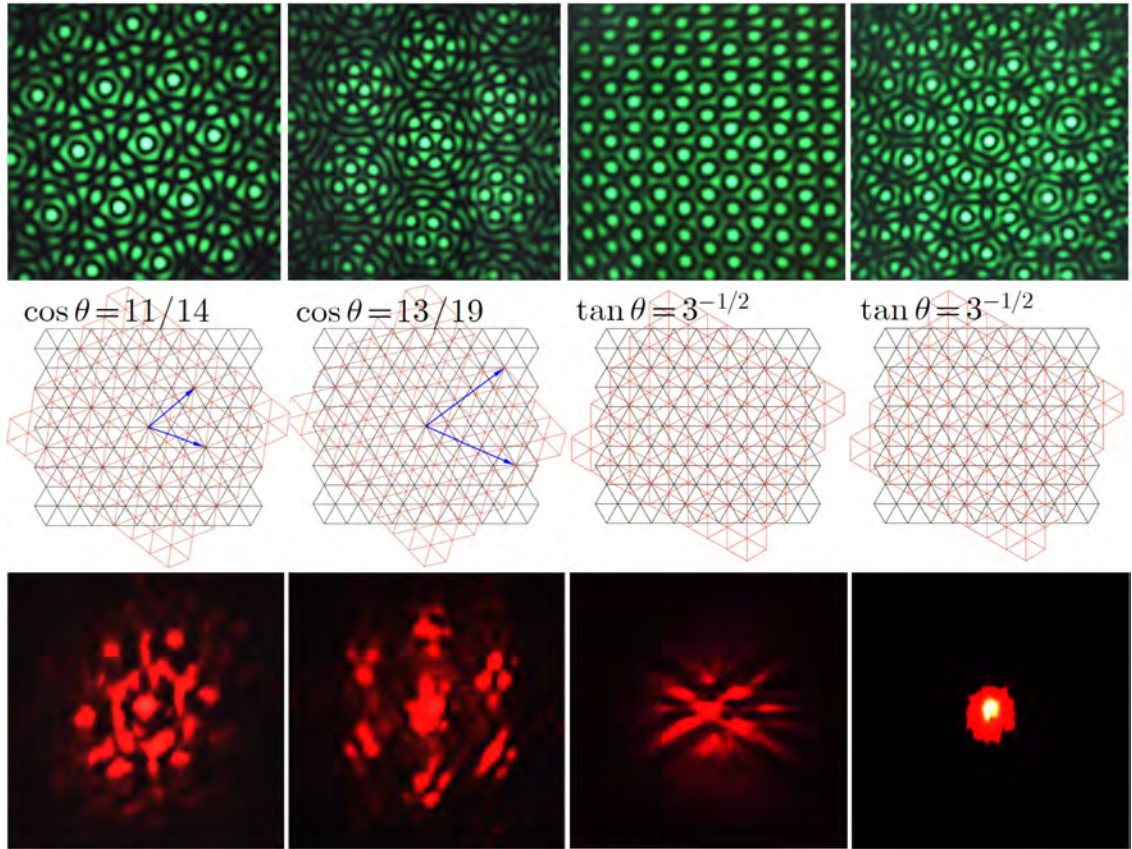
FIG. 4: First row: Moiré lattices produced by interference of two hexagonal patterns rotated by the angle θ: $p_2 = 1$ in the first, second, and fourth columns, while in the third column $p_2 = 0.18$. Second row: Schematic discrete representation of two rotated hexagonal sublattices. Third row: Measured output intensity distributions for signal beam at the output face of the crystal. In all cases $p_1 = 1$.

The moiré lattices can be created in practically any arbitrary configurations consistent with two-dimensional symmetry groups, thus allowing the creation of potentials that may not be easily produced in tunable form using material structures. In addition to the direct applications to the control of light patterns availability of the photonic moiré patterns allows the study of phenomena relevant to other areas of physics, particularly to condensed matter, which are harder to explore directly. An outstanding example is the relation between conductivity/transport and symmetry of incommensurable patterns with long-range

order. The concept can be also extended to atomic physics and in particular to Bose-Einstein condensates, where potentials are created using similar geometries (and where Anderson localization was already observed [35]). Finally, we note that while most previous studies of moiré lattices were focused on graphene and on quasicrystals, our results suggest that the photonic counterpart affords a powerful platform for the creation of synthetic settings to investigate wavepacket localization and flat-band phenomena in two-dimensional settings at large.

[1] Decker, R., Wang, Y., Brar, V. W., Regan, W., Tsai, H.-Z., Wu, Q., Gannett, W., Zettl, A. & Crommie, M. F. Local Electronic Properties of Graphene on a BN Substrate via Scanning Tunneling Microscopy, *Nano lett.* **11**, 2291-2295 (2011).

[2] Woods, C. R., Britnell, L., Eckmann, A., Ma, R. S., Lu, J. C., Guo, H. M., Lin, X., Yu, G. L., Cao, Y., Gorbachev, R. V., Kretinin, A. V., Park, J., Ponomarenko, L. A., Katsnelson, M. I., Gornostyrev, Yu. N., Watanabe, K., Taniguchi, T., Casiraghi, C., Gao, H-J., Geim, A. K. & Novoselov, K. S. Commensurate–incommensurate transition in graphene on hexagonal boron nitride, *Nat. Phys.* **10**, 451 (2014).

[3] Cao, Y., Fatemi, V., Demir, A., Fang, S., Tomarken, S. L., Luo, J. Y., Sanchez-Yamagishi, J. D., Watanabe, K., Taniguchi, T., Kaxiras, E., Ashoori, R. C. & Jarillo-Herrero, P. Correlated insulator behaviour at half-filling in magic-angle graphene superlattices, *Nature* **556**, 80 (2018).

[4] Cao, Y., Fatemi, V., Fang, S., Watanabe, K., Taniguchi, T., Kaxiras, E. & Jarillo-Herrero, P. Unconventional superconductivity in magic-angle graphene superlattices, *Nature* **556**, 43 (2018).

[5] Ahn, S. J., Moon, P., Kim, T.-H., Kim, H.-W., Shin, H.-C., Kim, E. H., Cha, H. W., Kahng, S.-J., Kim, P., Koshino, M., Son, Y.-W., Yang, C.-W. & Ahn, J. R. Dirac electrons in a dodecagonal graphene quasicrystal. *Science* **786**, 782-786 (2018).

[6] MacDonald, A. H. Bilayer Graphenes Wicked, Twisted Road, *Physics* **12**, 12 (2019).

[7] Bistritzer, R. & MacDonald, A. H. Moiré bands in twisted double-layer graphene, *PNAS* **108**,

12233-12237 (2011).

[8] Tarnopolsky, G., Kruchkov, A. J. & Vishwanath, A. Origin of magic angles in twisted bilayer graphene, *Phys. Rev. Lett.* **122**, 106405 (2019).

[9] Dean, C. R., Wang, L., Maher, P., Forsythe, C., Ghahari, F., Gao, Y., Katoch, J., Ishigami, M., Moon, P., Koshino, M., Taniguchi, T., Watanabe, K., Shepard, K. L., Hone, J. & Kim, P. Hofstadters butterfly and the fractal quantum Hall effect in moiré superlattices, *Nature* **497**, 598-602 (2013).

[10] San-Jose, P., González, J. & Guinea, F. Non-Abelian Gauge Potentials in Graphene Bilayers, *Phys. Rev. Lett.* **108**, 216802 (2012).

[11] Stampfli, P. A dodecagonal quasiperiodic lattice in two dimensional, *Helv. Phys. Acta* **59**, 1260-1263 (1986).

[12] Freedman, B., Bartal, G., Segev, M., Lifshitz, R., Christodoulides, D. N. & Fleischer, J. W. Wave and defect dynamics in nonlinear photonic quasicrystals, *Nature* **440**, 1166 (2006).

[13] Levi, L., Rechtsman, M., Freedman, R., Schwartz, T., Manela, O. & Segev, M. Disorder-enhanced transport in photonic quasicrystals, *Science* **332**, 1541 (2011).

[14] Huang, C., Ye, F., Chen, X., Kartashov, Y., Konotop, V. V. & Torner, L. Localization delocalization wavepacket transition in Pythagorean aperiodic potentials, *Sci. Rep.* **6**, 32546 (2016).

[15] F. Sgrignuoli, F., Wang, R., Pinheiro, F. A., & Dal Negro L. Localization of scattering resonances in aperiodic Vogel spirals. Phys. Rev. B **99**, 104202 (2019)

[16] Abrahams, E., Anderson, P. W., Licciardello, D. C. & Ramakrishnan, T. V. Scaling theory of localization: absence of quantum diffusion in two dimensions, *Phys. Rev. Lett.* **42**, 673-676 (1979).

[17] Brandes, T. & Kettemann, S. *The Anderson transition and its Ramifications-localization, quantum interference, and interactions* (Springer Verlag, Berlin, 2003).

[18] Mott, N. The mobility edge since 1967, *J. Phys. C: Solid State Phys.* **20**, 3075-3102 (1987).

[19] Aubry, S. & André, G. Analyticity breaking and Anderson localization in incommensurate lattices, *Ann. Israel Phys. Soc.* **3**, 133 (1980).

[20] Boers, D. J., Goedeke, B., Hinrichs, D. & Holthaus, M. Mobility edges in bichromatic optical lattices, *Phys. Rev. A* **75**, 063404 (2007).

[21] Modugno, M. Exponential localization in one-dimensional quasi-periodic optical lattices, *New J. Phys.* **11**, 033023 (2009).

[22] Li, C., Ye, F., Kartashov, Y. V., Konotop, V. V. & Chen, X. Localization-delocalization transition in spin-orbit-coupled Bose-Einstein condensate, *Sci. Rep.* **6**, 31700 (2016).

[23] Lahini, Y., Pugatch, R., Pozzi, F., Sorel, M., Morandotti, Davidson, R., N. & Silberberg, Y. Observation of a Localization Transition in Quasiperiodic Photonic Lattices, *Phys. Rev. Lett.* **103**, 013901 (2009).

[24] Roati, G., D'Errico, Fallani, C., L., Fattori, M., Fort, C., Zaccanti, M., Modugno, G., Modugno, M. & Inguscio, M. Anderson localization of a non-interacting Bose-Einstein condensate, *Nature* **453**, 895 (2008).

[25] Lüschen, H. P., Scherg, S., Kohlert, Th., Schreiber, M., Bordia, P., Li, X., Das Sarma, S. & Bloch, I. Single-particle mobility edge in a one-dimensional quasiperiodic optical lattice, *Phys. Rev. Lett.* **120**, 160404 (2018).

[26] Ye, L., Cody, G., Zhou, M., Sheng, P. & Norris, A. N. Observation of bending wave localization and quasi mobility edge in two dimensions. *Phys. Rev. Lett.* **69**, 3080-3083 (1992).

[27] Schwartz, T., Bartal, G., Fishman, S. & Segev, M. Transport and Anderson localization in disordered two-dimensional photonic lattices, *Nature* **446**, 52-55 (2007).

[28] Gauthier, R. C. & Mnaymneh, K. W. Design of photonic band gap structures through a dual-beam multiple exposure technique, *Opt. and Laser Techn.* **36**, 625 (2004).

[29] Fleischer, J., Segev, M., Efremidis, N. & Christodoulides, D. Observation of two-dimensional discrete solitons in optically induced nonlinear photonic lattices, *Nature* **442**, 147 (2003).

[30] Efremidis, N. K., Sears, S., Christodoulides, D, N., Fleischer, J. W. & Segev, M. Discrete solitons in photorefractive optically induced photonic lattices, *Phys. Rev. E* **66**, 046602 (2002).

[31] Suárez Morell, E., Correa, J. D., Vargas, P., Pacheco, M. & Barticevic, Z. Flat bands in slightly twisted bilayer graphene: Tight-binding calculations. *Phys. Rev. B* **82**, 121407 (2010).

[32] Franklin, P. The Elementary Theory of Almost Periodic Functions of Two Variables. *J. Math.*

Phys. **5**, 4054 (1926).

[33] Brouder, C., Panati, G., Calandra, M., Mourougane, C. & Marzar, N. Exponential localization of Wannier functions in insulators, *Phys. Rev. Lett.* **98**, 046402 (2007).

[34] Peleg, O., Bartal, G., Freedman, B., Manela, O., Segev, M. & Christodoulides, D. N. Conical diffraction and gap solitons in honeycomb photonic lattices, *Phys. Rev. Lett.* **98**, 103901 (2007).

[35] Billy, J., JosseV., Zuo, Z., Bernard, A., Hambrecht, B., Lugan P., Clément, D., Sanchez-Palencia1, L., Bouyer, P. & Aspect, A. Direct observation of Anderson localization of matter waves in a controlled disorder, *Nature* **453**, 891-894 (2008).

Author contributions   P. W. and Y. Z. contributed equally to this work. Experiments were conducted in Changzhi University. All authors contributed significantly to the paper.

Competing interests   The authors declare no competing interests.

METHODS

Experimental setup.   The experimental setup is illustrated in Extended Data Fig. 3. The lattice was created using optical induction, as described in [30] and first realized experimentally in [29]. A cw frequency-doubled Nd:YAG laser at wavelength $\lambda = 532$ nm is divided by a polarizing beam splitter into two *polarization* components, which are sent to Path **a** and Path **b** separately. Light in Path **a** is extraordinarily polarized and it is used to image the induced potential in the photorefractive crystal (see the third row of Fig. 1 in the main text). Light in Path **b** is ordinarily polarized and it is used to write the desirable potential landscape in the photorefractive SBN:61 crystal with dimensions $5 \times 5 \times 20$ mm^3 and extraordinary refractive index $n_{\mathrm{e}} = 2.2817$. Before entering the crystal ordinarily polarized light beam in Path **b** is modulated by Masks 1 and 2 transforming this beam into superposition of two rotated periodic patterns. Their relative strength p_2/p_1, or,

more precisely, the strength of the second lattice, as well as the twist angle θ are controlled by the polarizer-based Mask 1 and amplitude Mask 2. The He-Ne laser with wavelength $\lambda = 633$ nm shown in path **c** provides extraordinarily polarized beam focused onto the front facet of the crystal, that serves as a probe beam for studying light propagation in the induced potential. We record the output light intensity pattern by a CCD at the exit facet of the crystal after propagation distance of 20 mm.

Characteristics of moiré lattices used in experiment. In the experiments there have been used two types of moiré lattices, whose characteristics are summarized in Extended Data Table I. In all the cases the center of rotation in the (x, y) plane was chosen coincident with a node of one of the sublattices.

DATA AVAILABILITY

The data that support the findings of this study are available from the corresponding author F. Y. upon reasonable request.

EXTENDED DATA

Moiré lattice $I(\boldsymbol{r})$	Sublattice $V(\boldsymbol{r})$	Diophantine equation	$\tan \theta$
Pythagorean	$\cos(2x) + \cos(2y)$	$a^2 + b^2 = c^2$	b/a
hexagonal	$\sum_{n=1}^{3} \cos\left[2(x \cos\theta_n + y \sin\theta_n)\right]$	$a^2 + b^2 + ab = c^2$	$\sqrt{3}b/(2a + b)$

Extended Data Tab. I: Characteristics of the moiré lattices used in experiments. For hexagonal lattices $\theta_1 = 0$, $\theta_2 = 2\pi/3$, and $\theta_3 = 4\pi/3$.
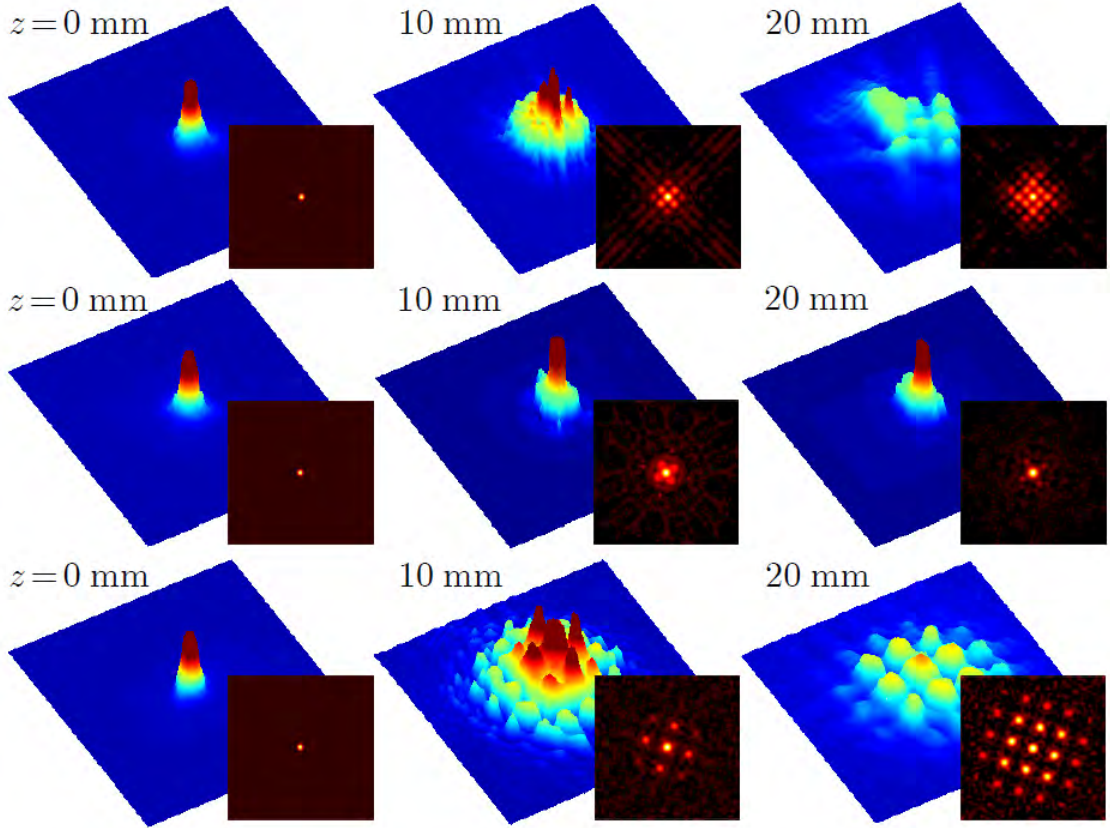
Extended Data Fig. 1: Experimentally observed intensity distributions of the probe beam (color-surface plots) and corresponding theoretically calculated distributions (insets), at different propagation distances z, for $\tan\theta = 3^{-1/2}$, $p_2 = 0.1$, which falls below the LDT point (top row), $\tan\theta = 3^{-1/2}$, $p_2 = 1$, which falls above LDT point (middle row), and $\tan\theta = 3/4$, $p_2 = 1$ (bottom row). The first two rows correspond to the incommensurable Pythagorean lattice shown in the central column of Fig. 1 of the main text. The third row corresponds to the commensurable lattice shown in the last column of Fig. 1 of the main text.

17
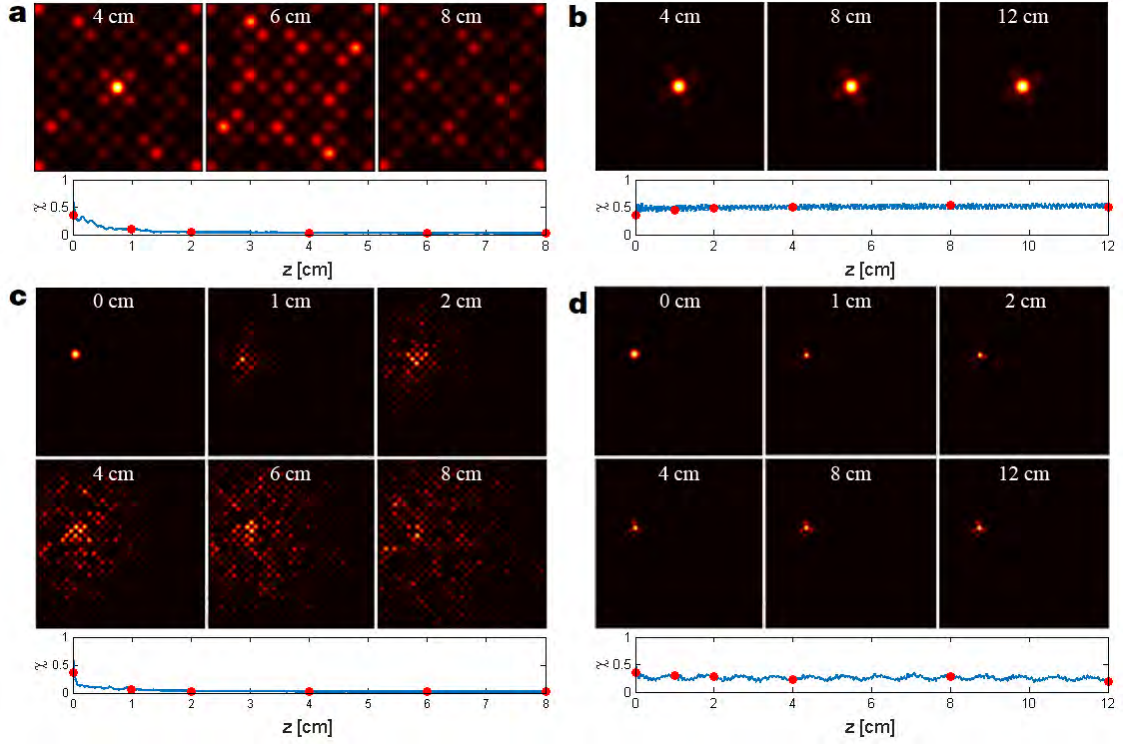
Extended Data Fig. 2: (a),(b) Numerical simulations of the light beam propagation in the incommensurable moiré lattice for central excitation, corresponding to top and middle rows of Extended Data Fig. 1, but for larger distances, notably exceeding sample length. (c),(d) Similar numerical results, but for off-center excitation position in moiré lattice. Parameter $p_2 = 0.1$ for (a),(c) and $p_2 = 1.0$ for (b),(d), while rotation angle $\theta = \pi/6$. In all cases Gaussian beam exciting a single site of the potential is assumed.
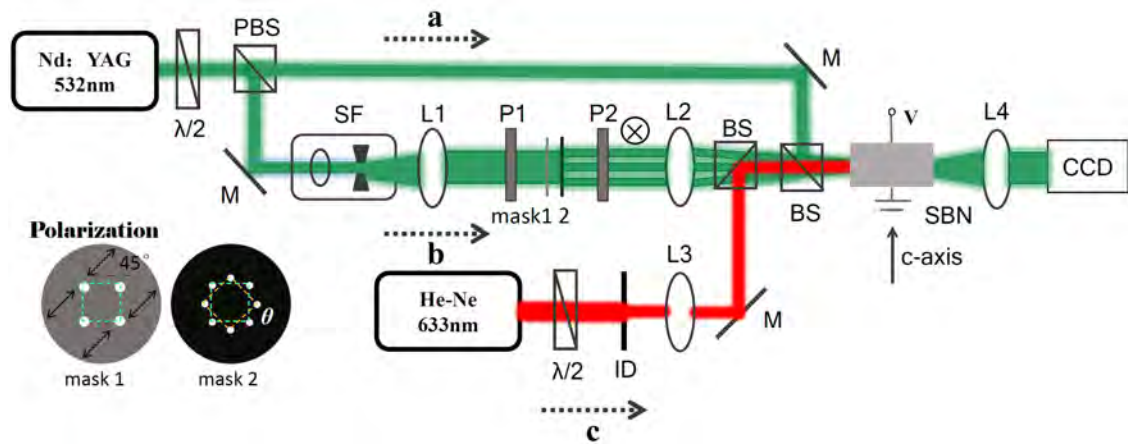
Extended Data Fig. 3: Experimental setup. $\lambda/2$, half-wave plate; PBS, polarizing beam splitter; SF, spatial filter; L, lens; BS, beam splitter; ID, iris diaphragm; M, mirror; P, Polarizer; SBN, strontium barium niobate crystal; CCD, charged-coupled device. Mask 2 is an amplitude mask to produce two group of sub-lattices with a rotation angle θ, and Mask 1 is made of a polarizer film.